Journal of Anatomy

J. Anat. (2011) **219**, pp259–272 doi: 10.1111/j.1469-7580.2011.01396.x

Using occlusal wear information and finite element analysis to investigate stress distributions in human molars

Stefano Benazzi,[1] Ottmar Kullmer,[2] Ian R. Grosse[3] and Gerhard W. Weber[1]

[1]*Department of Anthropology, University of Vienna, Vienna, Austria*
[2]*Department of Palaeoanthropology and Messel Research, Senckenberg Research Institute, Frankfurt am Main, Germany*
[3]*Department of Mechanical and Industrial Engineering, University of Massachusetts, Amherst, MA, USA*

Abstract

Simulations based on finite element analysis (FEA) have attracted increasing interest in dentistry and dental anthropology for evaluating the stress and strain distribution in teeth under occlusal loading conditions. Nonetheless, FEA is usually applied without considering changes in contacts between antagonistic teeth during the occlusal power stroke. In this contribution we show how occlusal information can be used to investigate the stress distribution with 3D FEA in lower first molars (M_1). The antagonistic crowns M_1 and P^2–M^1 of two dried modern human skulls were scanned by μCT in maximum intercuspation (centric occlusion) contact. A virtual analysis of the occlusal power stroke between M_1 and P^2–M^1 was carried out in the Occlusal Fingerprint Analyser (OFA) software, and the occlusal trajectory path was recorded, while contact areas per time-step were visualized and quantified. Stress distribution of the M_1 in selected occlusal stages were analyzed in STRAND7, considering occlusal information taken from OFA results for individual loading direction and loading area. Our FEA results show that the stress pattern changes considerably during the power stroke, suggesting that wear facets have a crucial influence on the distribution of stress on the whole tooth. Grooves and fissures on the occlusal surface are seen as critical locations, as tensile stresses are concentrated at these features. Properly accounting for the power stroke kinematics of occluding teeth results in quite different results (less tensile stresses in the crown) than usual loading scenarios based on parallel forces to the long axis of the tooth. This leads to the conclusion that functional studies considering kinematics of teeth are important to understand biomechanics and interpret morphological adaptation of teeth.

Key words: biomechanics; loading conditions; molars; occlusal wear pattern; three-dimensional finite-element analysis.

Introduction

In many studies, researchers have analysed the biomechanical effects of occlusal loads on teeth during clenching and mastication activities (e.g. Palamara et al. 2000; Dejak et al. 2003; Lucas, 2004). For functional reasons the external (i.e. the topography of the enamel cap) and internal architecture (i.e. enamel thickness and its microstructural organization) of a tooth must distribute the high stresses produced during masticatory loadings both in the teeth and in their supporting structure (Schwartz, 2000). Although the knowledge of these effects is important to understand the relation between functional demands and tooth morphology in an adaptive and evolutionary context (Macho & Spears, 1999), solutions to practical problems related to dental fracture mainly come from dentistry. An increased effort has been spent on dental prosthesis and endodontic treatments to test materials for tooth restoration and to explore the causes of dental failures. To evaluate the stress and strain distribution in teeth or dentures under loading conditions, several methods have been applied: electrical wire resistance strain gauge (Palamara et al. 2000; Prombonas & Vlissidis, 2002), photoelasticity (Fernandes et al. 2003) and, ultimately, finite element analysis (FEA) (De Jager et al. 2006; Jiang et al. 2010). The latter approach has generated increasing interest in dentistry. Nowadays, occlusal load simulations based on 2D or 3D FEA for testing different alternative materials are commonplace in dental industries (Cheng et al. 2010a; Fu et al. 2010).

Correspondence
Stefano Benazzi, Althanstraße 14, 1090 Vienna, Austria.
T: + 43 (01) 4277 54729; F: + 43 (01) 4277 9547; E: stefano.benazzi@univie.ac.at

Accepted for publication *22 April 2011*
Article published online *25 May 2011*

Nevertheless, there are several shortcomings in FEA modelling, which in the end confound a comprehensive understanding of functional biomechanics of teeth. Besides uncertainties regarding the load (bite force) that should be applied during these experiments, other important factors such as loading direction and loading position may be incorrectly defined (De Jager et al. 2005; Hattori et al. 2009). Whereas the patterns of stress distribution are not affected by the magnitude of load (Dejak et al. 2003; Jiang et al. 2010), they are affected by loading direction and position (De Jager et al. 2005; Fu et al. 2010). Until now in load experiments for molar tooth crowns, forces have usually been applied either parallel to the long axis of the whole tooth crown (Fu et al. 2010; Jiang et al. 2010), or oblique with respect to this axis, with a vector placed in the central basin (Ateş et al. 2006; Jiang et al. 2010), near the tip of the cusp (Palamara et al. 2002; Ateş et al. 2006; Coelho et al. 2009; Hasegawa et al. 2010; Rafferty et al. 2010), or in some other spots on the occlusal surface (Dejak et al. 2003; Nishigawa et al. 2003; De Jager et al. 2005, 2006; Fu et al. 2010). None of this work has considered the individual occlusal wear pattern when load directions and positions were specified.

Some researchers have emphasized this problem (e.g. Hattori et al. 2009), pointing out that during maximum intercuspation contact, wear facets in occlusal contact should be considered and loaded in different directions and to different extents. However, it is inaccurate and unrealistic to reduce the wear facets to point contacts (De Jager et al. 2006). Therefore, in some *in vivo* experimental tests occlusal contacts were registered during maximum clenching intensity using pressure-indicating film (Hattori et al. 2009; Kondo & Wakabayashi, 2009). This approach has the advantage of recording the occlusal loadings in maximum intercuspation at multiple occlusal contacts, but it still provides an incomplete picture of the real occlusal contact pattern during the complete sequence of the power stroke. Moreover, these general results cannot be used to interpret molar stress and strain pattern in extant or extinct primates other than living humans. To explore the biomechanical consequences of different tooth shapes and wear patterns and their variations within and between species, it is important to consider the occlusal relationships and crown morphology. Finally, results obtained by pressure-indicating film are limited to the maximum intercuspation contact during the power stroke. This represents a significant simplification because during the masticatory cycle the loads obviously vary due to the dynamically changing areas of contact.

Masticatory cycle

Mastication begins as a three-body interaction as the food is compressed between upper and lower teeth, flowing into the grooves and fissures of the dental crown and causing abrasion in the occlusal surface (DeLong, 2006). As soon as the food bolus is crushed and reduced to a thin film, attritional occlusal contacts occur between upper and lower dentition (two-body interactions), producing wear facets (Every, 1972; Kaidonis et al. 1993; Hillson, 2003; Kaidonis, 2008). In the initial closing phase of the jaw movements, food is placed between antagonistic teeth, acting to distribute the compressive forces on the occlusal surface, probably producing abrasive wear on cusp tips and the basin floors. During the tooth–tooth contacts on the attritional wear facet area, localized stress increases might be more damaging to the tooth crown than food–tooth contacts (Lucas, 2004). Consequently, it is important to identify the contact areas as they allow us to estimate how the chewing force is distributed in the tooth and in the supporting structure (DeLong, 2006).

The power stroke (or chewing phase) of mastication is divided into two phases: incursive (phase I) and excursive (phase II) (Hiiemae & Kay, 1972; Kay & Hiiemae, 1974). During the first part of the power stroke (phase I), the opposing molar crests tend to slide past each other, whereas beforehand cusp tips punctured and crushed the food. At the end of phase I, food is compressed between basins and cusps of molars. Phase II is described as an anterior-medial lower jaw movement, where the molars move out of occlusion and the jaws open. In phase II, food processing is described as grinding through the contacts between the wear facet areas at the lingual slopes of the buccal mandibular molar cusps and the buccal slopes of the lingual maxillary molar cusps. Accordingly, phase I and phase II are associated with shearing, crushing and grinding forces, respectively. Nonetheless, this concept has been recently questioned by Wall et al. (2006) based on data collected from an adult male *Papio anubis*. The authors verified that phase I movement is important as a grinding force, and proposed that phase II is less important than phase I for food breakdown.

Although uncertainties still persist about the relative contributions of phase I and phase II movements to food breakdown, there is agreement that these movements are distinct kinematic events (Wall et al. 2006). This results in a changing occlusal situation during a chewing sequence, so that '(T)he placement of wear facets across a tooth crown provides clues as to which phase of chewing occurs predominantly over a particular region of a cusp…' (Schwartz, 2000, 224). Accordingly, tooth wear pattern, including complementary wear facet pairs, offers details about occlusal movements between upper and lower crowns (e.g. Kullmer et al. 2009), without doubt providing additional information for improving load simulations (Molnar & Ward, 1977).

We can assume that tooth morphology is generally adapted to the loads the teeth undergo during their functional life (Spears & Macho, 1998; Macho & Spears, 1999). We propose here an approach towards a more realistic simulation of how chewing forces might be distributed

over tooth surfaces and how this would relate to wear areas. Although there are no *in vitro* or *in vivo* validation data available (and it is even unclear how such experiments could be set up), we think that our approach must lead to a more realistic loading scenario because it considers the mode of tooth loading based on a story that those teeth tell themselves (individual occlusal wear). In this contribution we raise two issues with regard to biomechanical analysis of teeth:

1 We present for the first time how individual occlusal information can be integrated with a biomechanical approach to investigate the stress distribution using 3D FEA in lower first molars (M_1) experiencing two-body interactions.

2 Our results provide three scenarios to be compared: the one mentioned above, considering the individual occlusal situation, and two more conventional analyses that involve loading the molar simply with parallel forces at two different areas of the central basin of the crown.

Materials and methods

Sample

Two dried modern human skulls from the Department of Anthropology, University of Vienna, were selected for the simulation. The sex and age at death were assessed by examination of the cranial and postcranial characters (Acsàdi & Nemeskéri, 1970; Ferenbach et al. 1980; Buikstra & Ubelaker, 1994). The first skull (ID = S23) is that of a young female (15–20 years old) from Africa. The second skull (ID = S138) is that of an adult male (30–40 years old) from Europe. The lower first molar (M_1) and the antagonistic upper second premolar (P^2) and first molar (M^1) were considered in the analysis. For S23, the right side (RM_1 and RP^2–RM^1) was chosen because it was in a better state of preservation. In S138, the right side was slightly damaged and the left side was used (LM_1 and LP^2–LM^1). The two specimens were selected because their M_1s differed in wear stage (after Smith, 1984): S23-RM_1 shows wear stage 2 (wear facets are visible on the occlusal surface, but without dentine exposure), whereas S138-LM_1 shows a wear stage between 3 and 4, with dentine exposed in the protoconid and entoconid cusps. The basic steps in our study are summarized in Fig. 1 and described in detail below.

Micro-CT scan, segmentation and 3D reconstruction

Scanning of both skulls with upper and lower dentition in maximum intercuspation contact was carried out at the Vienna Micro-CT Lab, Department of Anthropology, University of Vienna, with a Viscom X8060 μCT scanner using the following scan parameters: 130 kV, 100 mA, voxel length of 55 μm (S138) and 60 μm (S23).

The half-maximum height protocol (Spoor et al. 1993) was used to reconstruct 3D digital models for M_1 and the P^2–M^1 using the software package AMIRA 5.2 (Mercury Computer Systems, Chelmsford, MA, USA). This protocol samples the Hounsfield values on either side of the transition between two adjacent tissues and takes the value halfway between them as the threshold value. When voxels were located on the boundary between two tissues with similar Hounsfield values and the automatic threshold could not distinguish the differences, manual corrections were conducted.

For the M_1 (used for FEA, see below) a complete segmentation of the dental tissues (enamel, root and pulp chamber) and the underlying denture-bearing tissues (periodontal ligament – PDL, trabecular and cortical bone) was carried out (Fig. 2). To reduce the size of the digital models for FEA, we cut the mandibles distally to the socket of the lower second premolar and mesially to the socket of the lower second molar. Consequently, we considered only the bone tissues surrounding the M_1. For P^2–M^1, which were used to assess the occlusal contacts with M_1 (two-body interactions, see below). Only the external surface of the teeth was segmented. The final refinement of the digital models was carried out in RAPIDFORM XOR2 (INUS Technology, Inc., Seoul, Korea). Besides cleaning processes and corrections of defects to create fully closed surfaces, the digital models were optimized for downstream computer-aided engineering (CAE) applications.

Orientation of the specimens

A preliminary orientation of the digital models of both specimens in the Cartesian coordinate system was required before any further operation. In RAPIDFORM XOR2 the cervical lines of the M_1 were manually digitized using a curve, and a best-fit plane through the points of the curve was computed (cervical plane). Each specimen (including also P^2–M^1) was then rotated until the cervical plane of the M_1 was parallel to the *xy*-plane of the Cartesian coordinate system. Finally, the specimens were rotated along the *z*-axis until the mesial side of the M_1 was parallel to the *y*-axis.

Occlusal fingerprint analysis (OFA)

Occlusal fingerprint analyses of S23-RM_1 and S138-LM_1 were carried out to identify the contact areas (namely the wear facets) of the teeth being studied. Two OFA approaches were used to define 'loading position' and 'loading direction' for subsequent FEA in the M_1s: (i) a digital manual selection of the wear facets (facet mapping) on each M_1 occlusal surface (for more details of the method see Kullmer et al. 2009); (ii) a computer simulation of the interactions between M_1 and P^2–M^1 during the occlusal power stroke of the chewing cycle, using the OFA software, a virtual tool for the analysis of occlusal contact areas in antagonistic crown surface models through collision detection algorithms during simulation of occlusion.

Loading position

For digital facet mapping, each wear facet was manually marked in RAPIDFORM XOR2 by placing polylines onto the surface of the models (Ulhaas et al. 2004, 2007; Kullmer et al. 2009; Fiorenza et al. 2010). Wear facets were defined on the occlusal dental surface following the terminology of Maier & Schneck (1981), who identified a maximum of 13 complementary facet pairs on hominoid molars. The facets were divided into three groups: buccal phase I (blue), lingual phase I (green), and phase II (red) (Fig. 3).

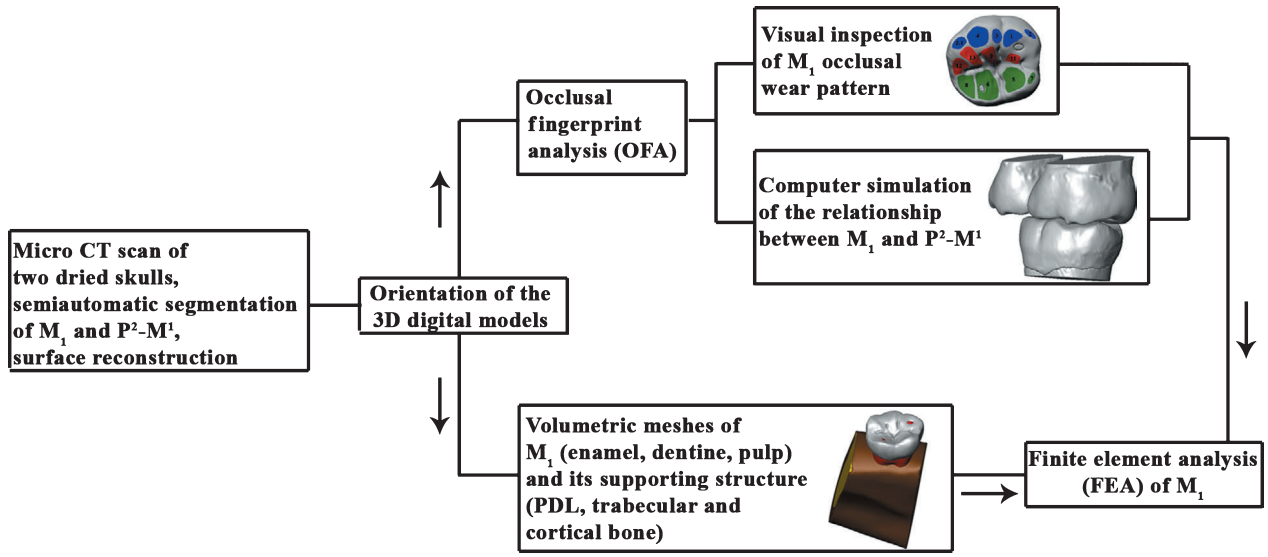

Fig. 1 Individual steps of the analysis.

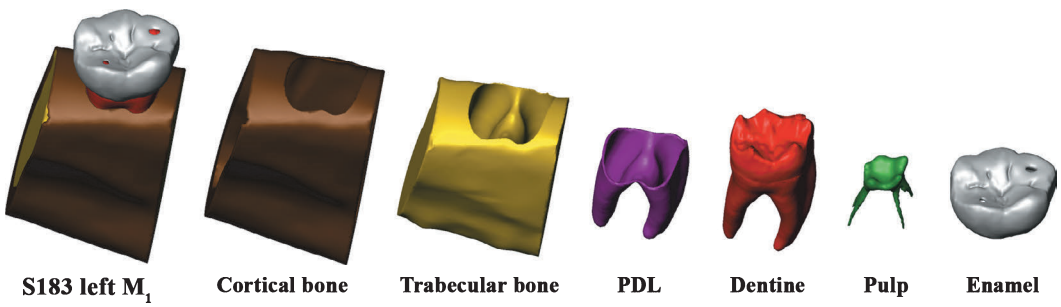

Fig. 2 Dental tissues and supporting structures for S138. PDL, periodontal ligament.

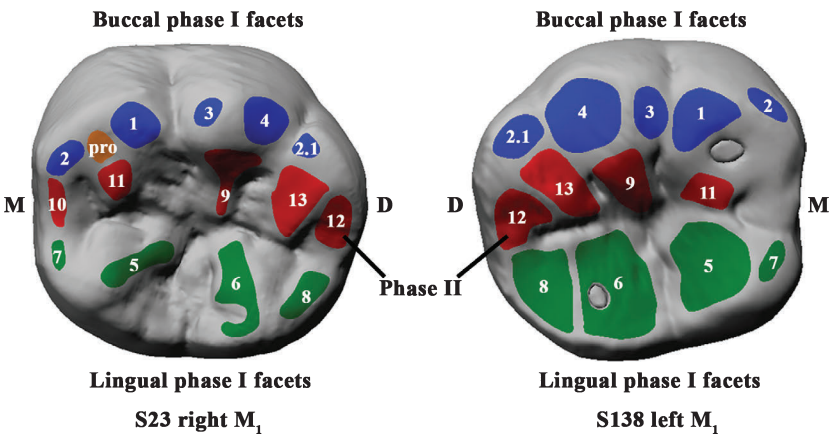

Fig. 3 Wear facets marked in S23-RM$_1$ (left) and S138-LM$_1$ (right). Wear facets are numbered after Maier & Schneck (1981), and divided into three groups: buccal and lingual phase I facets (blue and green, respectively) and phase II facets (red). A tip crush area is visible on the protoconid cusp (pro). D, distal; M, mesial.

The facet mapping yields a detailed picture of the occlusal wear pattern, but it does not indicate (i) whether the wear facets represent still active areas that experience chewing forces (the contact localities could have changed during wear processes) or (ii) the sequence of facet contacts during the power stroke (DeLong, 2006).

The OFA software analyses the occlusal approaches of the wear facets during phase I and phase II. The OFA reconstructs the occlusal pathway of antagonistic teeth through collision detection of virtual surface models, providing a sequence of selected surfaces, including contact area quantification (Fig. 4). This permits the interpretation of the progress of occlusal

contacts during phase I and phase II movements. The visualization of the spatial position and size of contacts during phase I, centric occlusion and phase II was used to compute the load directions and exact locality on the tooth crown for the FEA.

Loading direction

The loading direction changes during the masticatory cycle depending on the chewing phase. For maximum intercuspation contact we can assume that a compressive force acts between complementary wear facet pairs, which can be represented as perpendicular loads to these facets (Hattori et al. 2009). Accordingly, in RAPIDFORM XOR2 we created the best-fit planes for each wear facet and computed the normal vectors of each facet plane (Fig. 5A), which is used to specify the direction of the compressive normal force applied to each facet.

For phase I and phase II, besides the normal force the tangential force at the surface opposite to the direction of sliding motion should be considered to load the tooth. The latter is due to the relative sliding motion of the M_1 with respect to the antagonistic teeth. The OFA software provides the direction of sliding motion, namely the trajectory of the lower molar during the chewing sequence (Fig. 5B). For each facet of phase I and phase II we computed the resultant force direction between the directions of the normal force and the tangential force (Fig. 5C). The tangential force is given by the coefficient of friction times of the normal force. As an example, Fig. 4C shows the computation of the resultant force direction for wear facet 2.1 during phase I. Several *in vitro* experiments have been carried out by researchers to determine the coefficient of friction for human and non-human enamel as well as for other restorative materials (e.g. Reeh et al. 1995; Zheng & Zhou, 2006, 2007; Roy & Basu, 2008). There is a large variation in the coefficient of friction (from 0.1 to 0.7), which is strongly related to (i) the progressive increase of wear in the tooth (as a function of number and direction of chewing cycles), (ii) the mechanical properties, microstructure, chemical compositions of teeth and (iii) the wear test parameters used (i.e. wet or dry enamel) (DeLong, 2006; Zheng & Zhou, 2006). We used a coefficient of friction of 0.2, which was found for wet conditions (Li & Zhou, 2002). Because this value is not undisputed (DeLong, 2006), we note that the results in phase I and phase II would be different using other estimations for the coefficient of friction.

Finite element mesh generation and FEA

The surface models were then imported into STRAND7 Software (G+D Computing Pty Ltd, Sydney, NSW, Australia), where volumetric meshes of S23-RM_1 and S138-LM_1 (including PDL, cortical and trabecular bone shown in Fig. 2) were created initially using four-noded tetrahedral elements. The specimens were analysed, and then reanalysed using 10-noded tetrahedral elements to ensure convergence in the pattern of stress. We were therefore confident that the discretization error due to the representation of the continuum with a finite number of elements was well enough controlled to compare the various load cases. As a result, the first specimen (S23) was meshed with a total of 692 732 nodes and 482 962 10-noded tetrahedral elements, and the second specimen with a total of 775 442 nodes and 536 769 10-noded tetrahedral elements (Fig. 6A).

Information about material properties (the elastic modulus – E, and the Poisson's ratio) was collected from the literature and is summarized in Table 1. All materials used in the models were considered homogeneous, linearly elastic and isotropic, assumptions that are regularly applied with simpler continuum mechanics models (e.g. Dejak et al. 2003; De Jager et al. 2005, 2006; Chowdhary et al. 2008; Gurbuz et al. 2008; Coelho et al. 2009; Fu et al. 2010; Jiang et al. 2010).

Boundary constraints were applied to the lower border of the mandible, and all the associated nodes were fully restrained (Fig. 6B). To check whether results could be affected by different boundary conditions, a further FEA was carried out restraining both the lower border of the mandible and all of the nodes on the mesial and distal aspect of the mandible models. No differences in outcomes were observed between the two boundary constraints.

A load of 75 N was applied for phase I, 150 N for maximum intercuspation contact in the direction of the long axis of the tooth, and 75 N again for phase II. For maximum intercuspation contact, 150 N is an average force found in the literature for loading conditions (Palamara et al. 2000; Dejak et al. 2003; Cheng et al. 2010b; Fu et al. 2010). There is little information in the literature about the appropriate loads for phase I and phase II. As mentioned above, Wall et al. (2006) proposed that phase II movement has a less significant role in food breakdown than phase I movement. Although there are no measurements available, it is reasonable to assume that during phases I and II, the forces involved are lower than those produced during maximum intercuspation contact (150 N). As a rough estimate for our simulation we decided to use half of the force for phases I and II

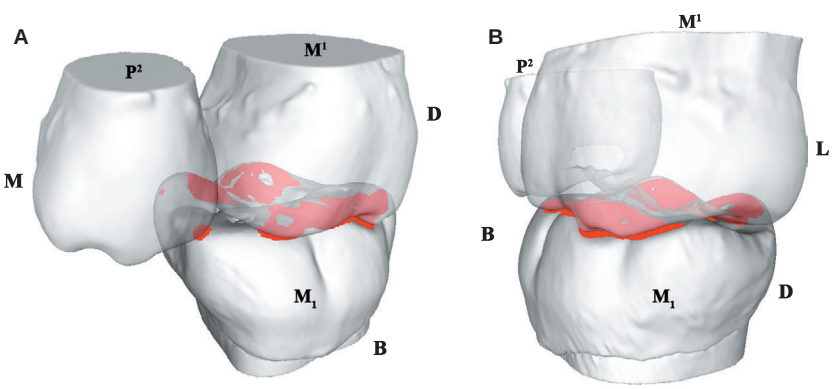

Fig. 4 Collision detection for specimen S138 in the Occlusal Fingerprint Analyser software (OFA) during a representative time-step of phase I. The LP^2–LM^1 are transparent to show the collision (red spots) in the occlusal surface of the LM_1. (A) mesiobuccal view. (B) distobuccal view. B, buccal; D, distal; L, lingual; M, mesial.

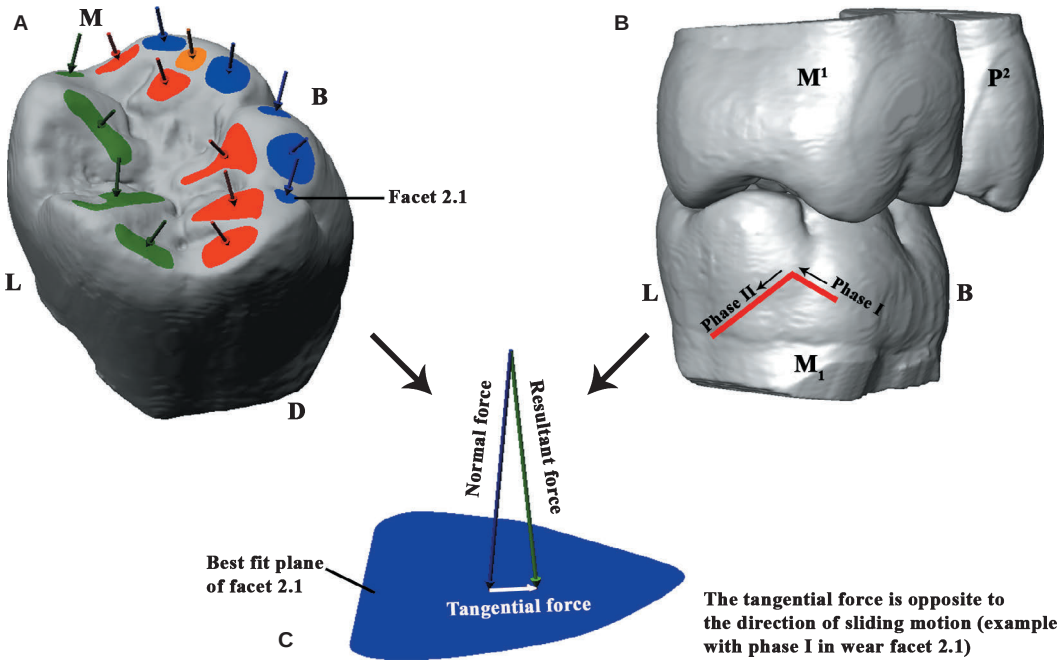

Fig. 5 S23 specimen. (A) S23-RM$_1$ shows the normal vectors of each facet's plane. Wear facets and normal vectors are divided into three groups: buccal and lingual phase I facets (blue and green, respectively) and phase II facets (red). To simplify the picture, only a vector has been shown for each facet's plane. Nevertheless, for maximum intercuspation contact, as well as for phase I and phase II, the pressure was applied on all tetrahedral faces included in the contact area. (B) Maximum intercuspation contact between M$_1$ and the antagonistic teeth P^2 and M^1. The medial movement of M$_1$ during both phase I and phase II is displayed in red. (C) Resultant force between the normal force and the tangential force for facet 2.1 (phase I). B, buccal; D, distal; L, lingual.

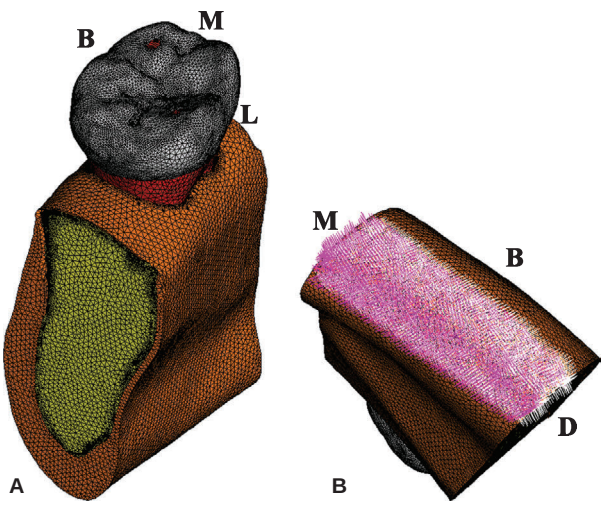

Fig. 6 Specimen S138. (a) The FE mesh consisting of 536 769 ten-noded tetrahedral elements. (b) The fully restraint nodes in the lower border of the mandible are displayed in pink/white colors. B, buccal; D, distal; L, lingual; M, mesial.

(75 N). These values are uncertain but our goal here was to detect patterns of stress distribution in the M$_1$ (which is not affected by the loading value because at each material point of the model the stress is linearly proportional to the force

Table 1 Elastic properties of isotropic materials.

Material	E* (Gpa)	Poisson's ratio	Reference
Enamel	84.10	0.30	Magne (2007)
Dentine	18.60	0.31	Ko et al. (1992)
Pulp	0.002	0.45	Rubin et al. (1983)
PDL**	0.0689	0.45	Holmes et al. (1996)
Alveolar bone	11.50	0.30	Dejak et al. (2007)
Cortical bone	13.70	0.30	Ko et al. (1992)

*Elastic modulus.
**Periodontal ligament.

applied) rather than to predict realistic loads that cause, for example, fractures of the tooth enamel.

For each phase, including the maximum intercuspation contact, the load was distributed proportionally according to the contact area of the wear facets involved. Therefore, for each phase all facets in contact were subjected to a uniform pressure (i.e. a distributed load), and these pressures were applied on all tetrahedral faces included in the contact area. STRAND7 uses these pressures to calculate a set of 'consistent' nodal forces that are applied to the nodes in the contact area. Consistent nodal forces conserve both the total force and the work of the pressure load (Cook et al. 2002). For the maximum intercuspation phase, the pressure load normally applied to the contacting facets was such that the net

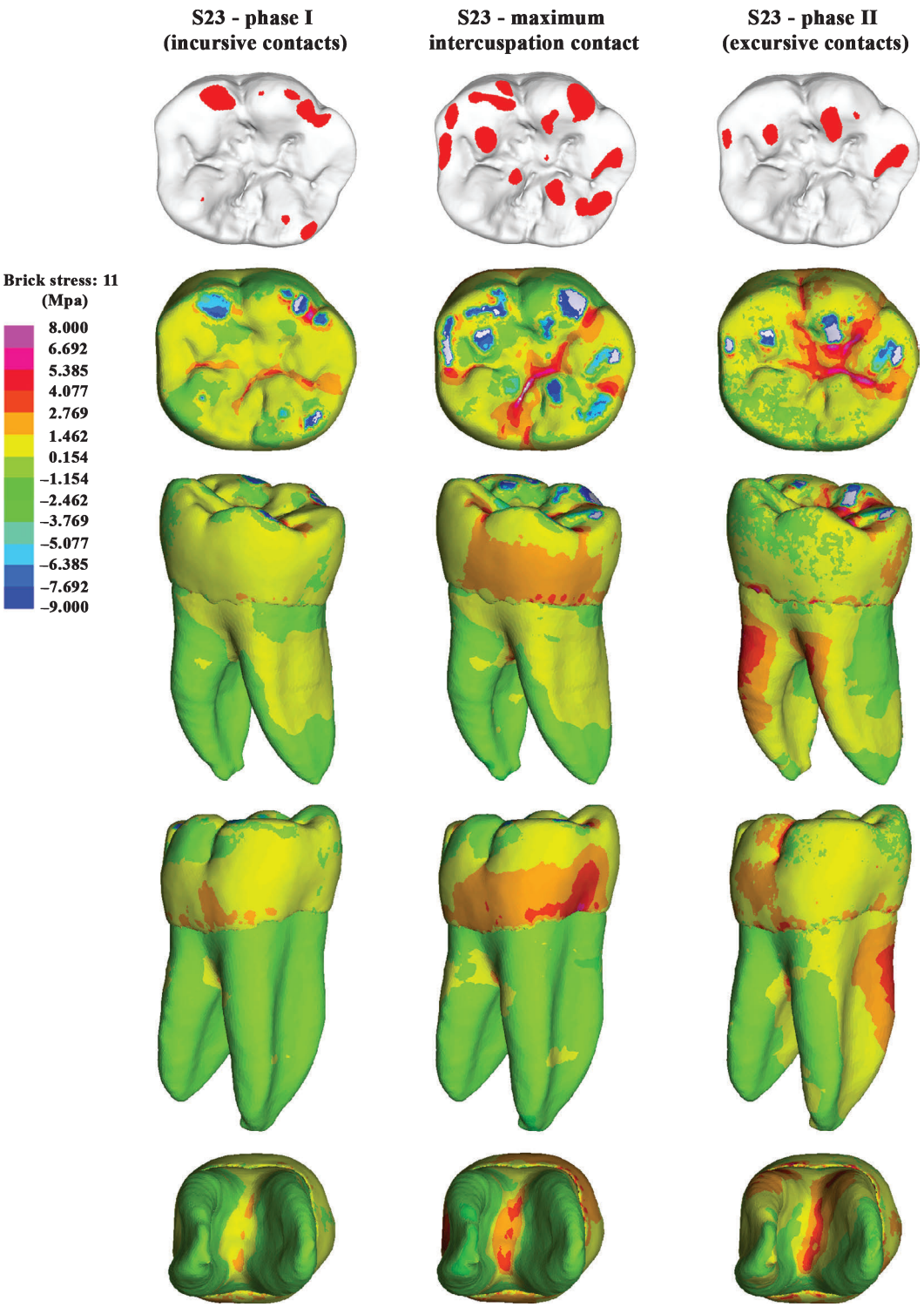

Fig. 7 S23-RM_1 specimen. Occlusal contacts detected by the Occlusal Fingerprint Analyser software (first row). Three occlusal time steps (phase I, maximum intercuspation and phase II respectively) were chosen for FEA. Second row, occlusal view; third row, distolingual view; fourth row, mesiobuccal view; fifth row, apical view. Red spots in the RM_1 of the first row represent the contact areas with the antagonistic teeth. Gray areas in the FEA results account for maximum principal stresses less than the user range limit.

component of force applied in the direction of the long axis of the tooth was 150 N, in order to compare to the simplified conventional tooth load cases discussed below.

Information about 'loading position' and 'loading direction' (direction of the force for each wear facet), were obtained from static OFA (see above). For phase I and phase II we selected two

representative time-steps where most of the facet areas of each phase are in occlusal contact.

For both specimens we computed the long axis of the M_1 in RAPIDFORM XOR2. For comparative purposes, two further FEAs were carried out loading the M_1 with parallel forces only (150 N) to the longitudinal axis of the tooth: (i) the load was concentrated onto a single point at the central basin of the crown (PAR-POINT); (ii) the load was distributed over a larger area of the central basin (PAR-AREA).

As brittle fracture represents the common failure mode of dentures, the stress patterns were formed according to the maximum principal stress criterion for brittle materials (Cheng et al. 2010a; Hasegawa et al. 2010). In fact, both dentine and, in particular, enamel have a much lower resistance to tension than to compression across prisms (Dejak et al. 2005). The maximum principal stress is presented graphically as stress distribution maps. Areas shown in purple have the highest tensile stresses, whereas blue areas have the lowest value for maximum principal stress. If this value is negative, then all three principal stresses are negative (i.e. compressive) at this point, and the material is therefore in a state of triaxial compression. For each specimen we set the range limits of the colour maps to allow intra-specimen comparison of the stress distribution among phases. White or off-white colours indicate values of maximum principal stress less than or greater than the user-specified limits, respectively.

Results

S23 specimen

Occlusal contact information obtained using the OFA software is shown in the first row of Fig. 7. The same figure provides the distribution of maximum principal stress in phase I, maximum intercuspation contact and phase II respectively. The stress distribution changes in the tooth during the chewing phases. In phase I, due to forces applied in wear facets 1, 2.1, 3, 4, 5, 6 and 8 (see also Fig. 3), tensile stresses are located in the central basin of the crown and in the distobuccal groove that separates the hypoconid and hypoconulid cusps.

In maximum intercuspation the contact areas increased both in number and extension. Tensile stresses are observed in the grooves of the occlusal surface, especially in the lingual groove separating the metaconid and entoconid, and in the distobuccal groove between hypoconid and hypoconulid. Moreover, tensile stresses extend up to the mesial and distal marginal ridge, as well as in the distal and especially in the mesial lower third of the crown. The root is basically subjected to compressive stresses, except at the base of the root bifurcation. In phase II the forces were applied in wear facets 9, 10, 11, 12 and 13, which cause tensile stresses in the distal half of the mesiodistal groove of the occlusal surface and in the grooves separating the buccal cusps (protoconid/hypoconid and hypoconid/hypoconulid). High tensile stresses are also observed in the lingual aspect of the roots and at the base of the root bifurcation. In all three cases, tensile stresses converge in the grooves and fissures between the ridge crests on the occlusal surface.

The pattern of stress distribution observed in the enamel–dentine junction (EDJ) confirms that during maximum intercuspation contact, the tooth is subjected more to compressive than to tensile stresses (Fig. 8). In phase I, and mainly in maximum intercuspation, the greater tensile stresses are observed in the grooves and crests between the buccal horns. In phase II, the EDJ is subjected to tensile stresses in the groove between the buccal horns (especially the distobuccal horns) as well as in the buccal slope of the distolingual horn.

Results obtained by loading the molar in the occlusal basin (PAR-POINT and PAR-AREA) differ from those obtained by loading the molar on the occlusal contact areas (Fig. 9). The huge areas of tensile stresses with parallel loading conditions are striking in comparison with the OFA-driven simulation. Note the large areas of the occlusal surface affected by tensile stresses and high tensile stresses appearing at the lower third of the crown for the parallel loadings (Figs 7 and 9).

S138 specimen

The results of the three loading conditions (for phase I, maximum intercuspation contact and phase II) for specimen

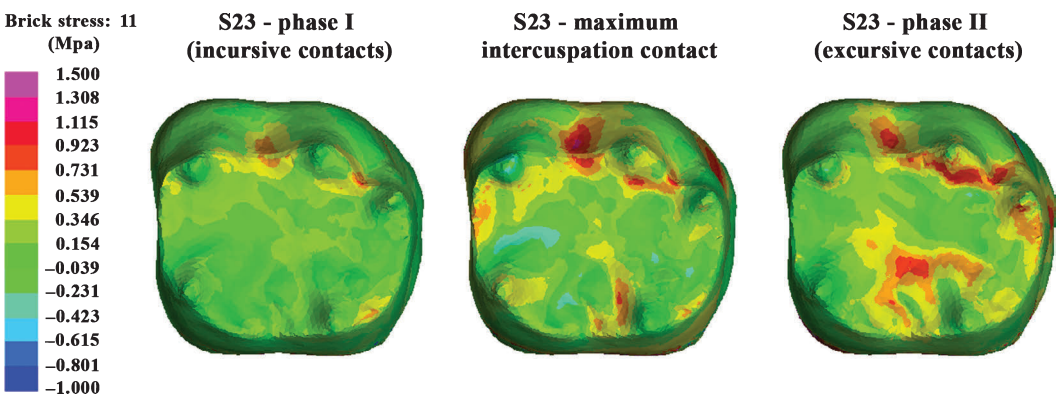

Fig 8 S23-RM_1 specimen. Maximum principal stress distribution in the EDJ for phase I, maximum intercuspation contact and phase II respectively.

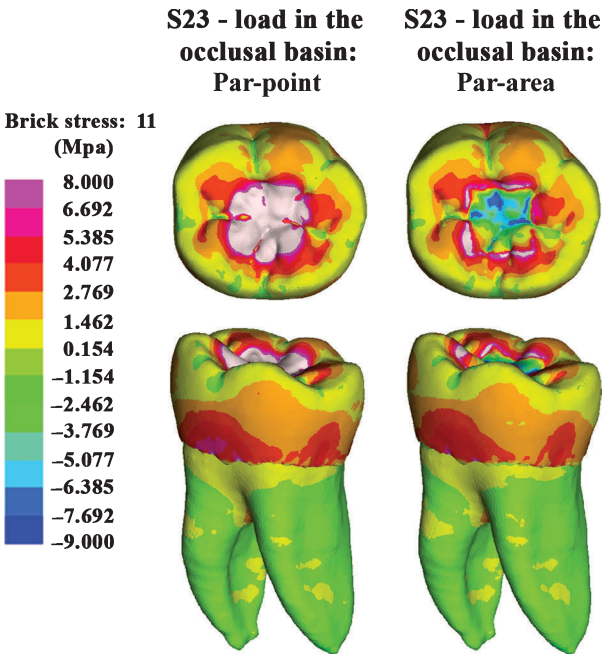

Fig. 9 S23-RM_1 specimen. Maximum principal stress distribution observed when the tooth is loaded (i) onto a single contact point of the occlusal basin (left, PAR-POINT); and (ii) onto a larger area of the occlusal basin (right, PAR-AREA). First row, occlusal view; second row, distolingual view. Grey or off-grey areas in the FEA results indicate maximum principal stresses larger than the user-specified limits.

S138 are shown in Fig. 10. In phase I, forces were applied in wear facets 1, 2.1, 3, 4, 5, 6 and 8. Tensile stresses are mainly located in the central basin of the crown (in the mesiodistal groove) as far as the distal marginal ridge and in the groove separating the two lingual cusps. The root is essentially subjected to compressive stresses.

During maximum intercuspation contact, tensile stresses affect the central basin of the crown, the groove separating the two lingual cusps, the lingual wall of the crown under the metaconid cusp, the mesial and distal lower third of the crown, and the base of the root bifurcation. In phase II, tensile stresses are located in the central basin of the crown, in the buccal groove separating the two principal cusps, slightly in the distal lower third of the crown, in the lingual aspect of the root (in particular the mesial root) and at the base of the root bifurcation.

The EDJ is basically subjected to compressive stresses. Nonetheless, during maximum intercuspation contact, high tensile stresses were observed in the grooves and the crests connecting the buccal dentine horns and in the distal marginal ridge (Fig. 11). To a lesser extent, the same tensile stress distribution occurred in phase II. Phase I also shows tensile stresses in the crests adjacent to the distolingual horn (entoconid).

Loading the molar in the central basin, either with a point load (PAR-POINT) or with a more distributed load (PAR-AREA), causes high tensile stresses again on the occlusal surface of the crown and in the lower third of the crown, but the stresses in this tooth are more concentrated near the cervix (Fig. 12). As in the previous experiment with a less worn tooth (S23), tensile stresses under parallel loading conditions are much higher on the occlusal surface than those observed for the OFA-driven approach during maximum intercuspation contact (Figs 10 and 12).

Discussion and Conclusions

During food breakdown, abrasion occurs on the occlusal surface of teeth due to food placed between upper and lower dentition (Kay, 1977). Accordingly, compressive forces are spread over all the occlusal surfaces due to the interposition of food bolus (three-body interactions). As soon as the food bolus is reduced to a thin film, attritional occlusal contacts occur between antagonists. The compressive forces experienced by the teeth during these contacts (two-body interactions), along with their relative sliding motion, produce attritional wear facets. Accordingly, it appears to be an oversimplification to reduce forces to a point load placed, for example, in the central basin, a scenario that has often been employed in biomechanical studies of teeth (e.g. Ateş et al. 2006; Hasegawa et al. 2010; Jiang et al. 2010). A point load does not exist in the physical world, and mathematically results in a singularity in stress and strain tensor at the location of the point load, which in an FE model produces an artificially high stress and strain that only increases as the mesh is refined (Turteltaub & Sternberg, 1968; Cook et al. 2002). Applying pressure loads normal to contact surfaces and frictional loads distributed over the contact areas and in the opposite direction to motion is fully consistent with the basic mechanics of contacting bodies. The value we used is somewhat arbitrary, but the magnitude of load does not affect patterns of stress and strain, which is what we are comparing. Although we lack experimental data from *in vivo* or *in vitro* validation at this point, we argue that our approach is a step towards developing a more realistic scenario for tooth biomechanics because it considers the power stroke kinematics of occluding teeth experiencing two-body interactions.

The results presented in this pilot study are only preliminary ones to demonstrate the potential of this combined OFA and FEA approach. A much larger sample size, more data on loads employed and validation of results are needed. Nevertheless, some interesting observations can be made even in this early stage.

1 In previous work it was suggested that, at least for mandibular premolars, the marginal ridges are not exposed to high stress during point occlusal loading due to their greater thickness of enamel compared with other areas (Palamara et al. 2002). Nevertheless, the authors admitted that point loading could not correctly reflect normal occlusal loading, advising also that cusps

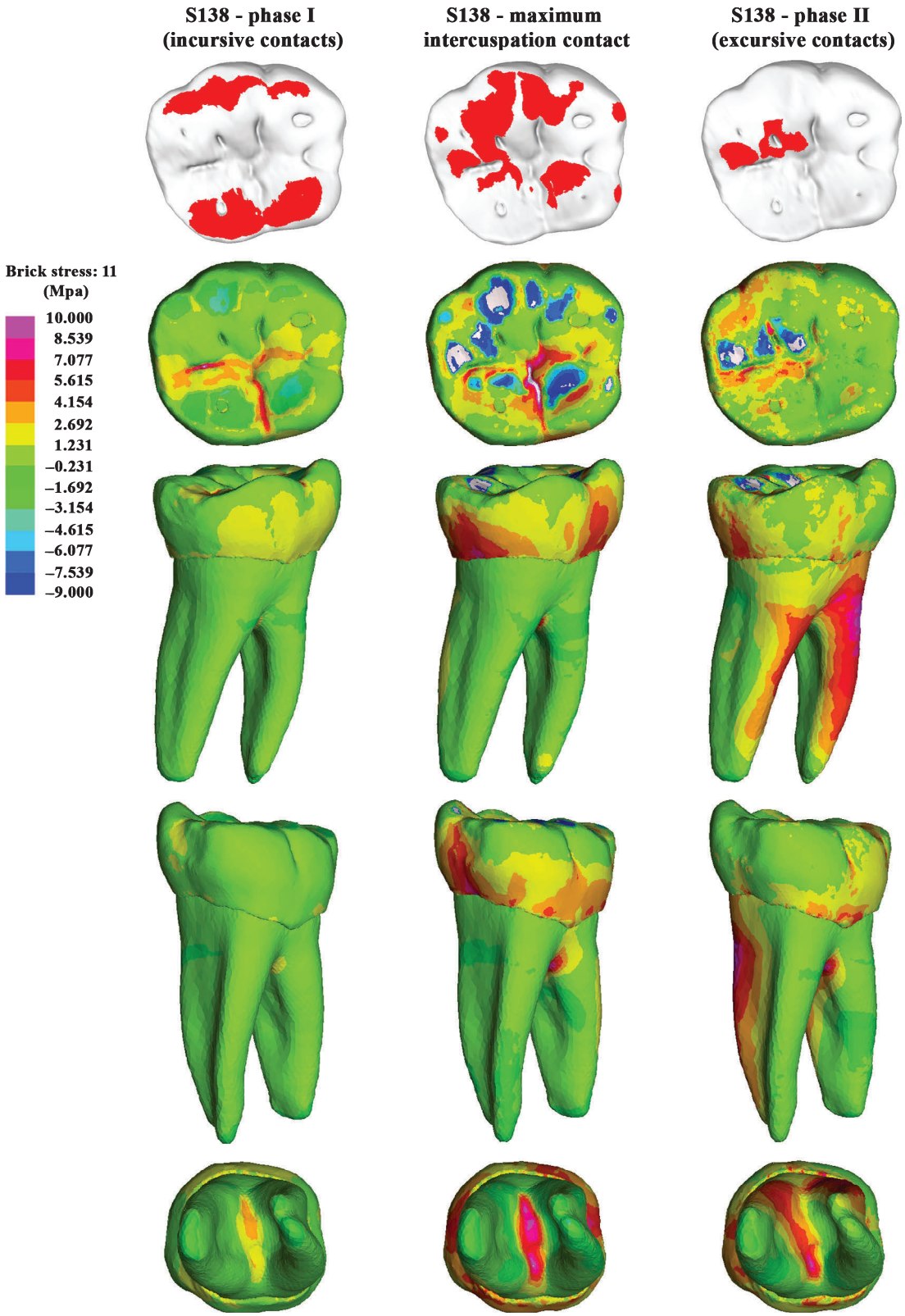

Fig. 10 S138-LM_1 specimen. Occlusal contacts detected by the Occlusal Fingerprint Analyser software (first row). Three occlusal time steps (phase I, maximum intercuspation and phase II, respectively) were chosen for FEA. Second row, occlusal view; third row, distolingual view; fourth row, mesiobuccal view; fifth row, apical view. Red spots in the LM_1 of the first row represent the contact areas with the antagonist teeth. Grey or off-grey areas in the FEA results indicate maximum principal stresses less than or larger than the user-specified limits, respectively.

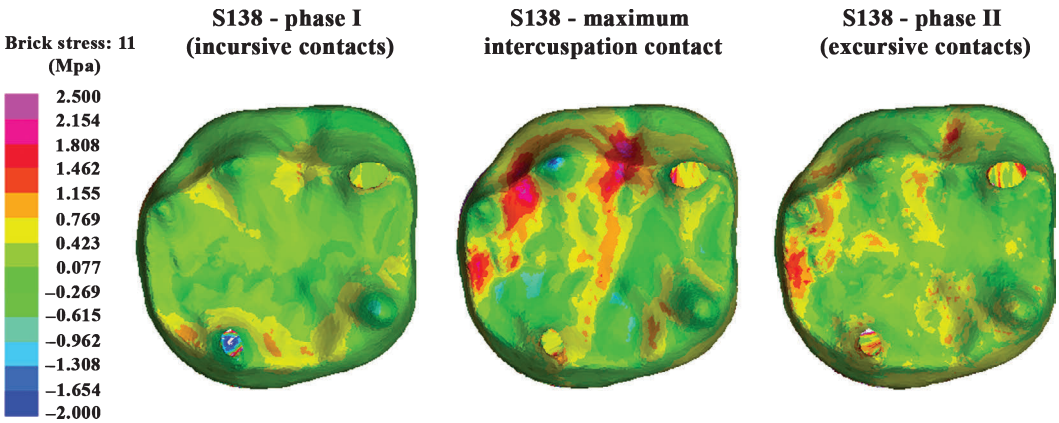

Fig. 11 S138-LM$_1$ specimen. Maximum principal stress distribution in the EDJ for phase I, maximum intercuspation contact and phase II, respectively.

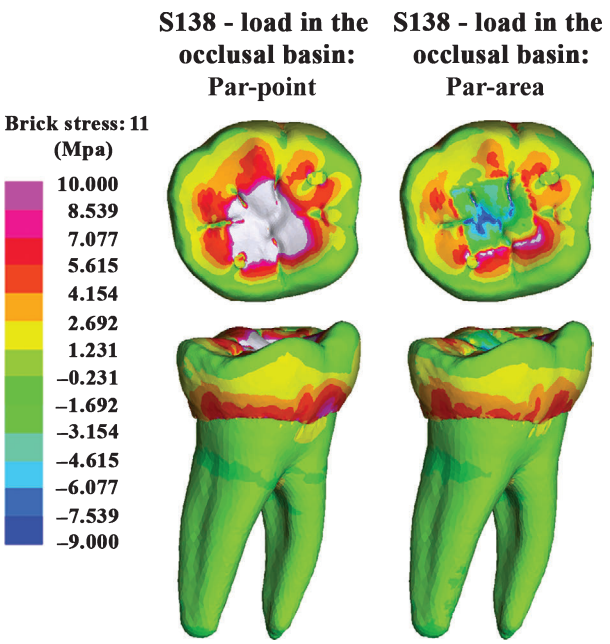

Fig. 12 S138-LM$_1$ specimen. Maximum principal stress distribution observed when the tooth is loaded (i) onto a single contact point of the occlusal basin (left, PAR-POINT), and (ii) onto a larger area of the occlusal basin (right, PAR-AREA). First row, occlusal view; second row, distolingual view. Grey or off-grey areas in the FEA results indicate maximum principal stresses larger than the user-specified limits.

of antagonistic teeth could directly contact (thus creating wear facets) the marginal ridge (Palamara et al. 2002). Our results indicate that marginal ridges might be highly stressed areas, at least in M$_1$s (see Fig. 7).

2 It has also been suggested that high values of strain are usually concentrated near the cervix, both for the enamel and the dentine (Palamara et al. 2000). Regarding the enamel, several reasons were proposed such as the weaker bond between enamel and dentine at the cervix and also because of the thinner enamel in that region (Goel et al. 1991). Moreover, Chowdhary et al. (2008) observed that tensile stresses are distributed in the buccal lower third of the M$_1$ crown. Our observations for maximum intercuspation contact, both for S23 and S138, show tensile stresses in the lower third of the mesial and distal sides of the crown, but cannot confirm those on the buccal side. We have also shown that when the forces are distributed according to our OFA-driven approach, much less stress is recorded at the lower third of the crown compared to the high tensile stresses obtained when the more unrealistic parallel loads are applied in the occlusal basin.

3 For both specimens, at least during maximum intercuspation, high tensile stresses were observed at the base of the root bifurcation. As root form and size should reflect both bite force potentials and tooth use (Kupczik & Hublin, 2010), this could explain the more apically positioned furcation – and often fused roots – observed in Neanderthals in contrast to modern human mandibular molars. Previous studies suggested that Neanderthals were capable to resist larger occlusal forces than recent modern human (Kupczik & Hublin, 2010). Accordingly, an elongated root body with short root branches could reduce the tensile stresses produced at the base of the root bifurcation during maximum intercuspation contact.

4 Little information is available in the literature about the functional importance of grooves, fissures and crests on the occlusal surface and on the EDJ. Our results suggest that grooves and fissures are critical locations, as tensile stresses are concentrated at these features. This leads us to the hypothesis that they might act to increase the structural stiffness of the tooth locally, thereby directing more of the applied load through the centre portion of the crown and reducing the general stresses in the tooth elsewhere. To prove this, it will be necessary to compare results under identical load conditions for tooth morphologies that show marked grooves

and fissures and that do not. With regard to this, several future investigations will be developed using this approach to assess the functional utility of some occlusal features in extant and extinct primate taxa.

5 Finally, the combination of FEA and OFA provides new insights about how changing force distributions during occlusion might explain the creation of interproximal wear facets. Interproximal tooth wear is the result of tooth-to-tooth contact and crown movements occurring during the chewing cycle or other non-masticatory activities. Two main forces are involved during masticatory movements: a lateral force that directs buccolingually and mesial force vectors that push the teeth to migrate anteriorly (Picton, 1962). In our example, the buccolingual displacement could be recognized for both the specimens in phase II. The forces applied in the lingual slope of the buccal cusps cause a buccal displacement of the crown and the concomitant tensile stress in the lingual wall of the roots. Further studies that consider the neighbouring teeth – and not just antagonistic tooth pairs – are required to better elucidate the dynamic involved in the creation of interproximal wear facets.

6 For the interpretation of the results of this study we acknowledge some limits that need to be addressed in future investigations. (i) The preparation of data as well as the OFA and FEA involve a huge labour effort and advanced software tools and application know-how, which restricts the sample size at the moment considerably. However, with the increasing dispersion of tools and growing computer power these limitations will be less important within the next years. (ii) Besides our small sample size in this pilot study, we emphasize that there is uncertainty about the applied forces for phase I and phase II, as well with regard to the value of the coefficient of friction for computing the tangential force; we hope that our contribution will stimulate more research in these directions. (iii) In our study we have not considered the temporary effect of the various chewing events or the biomechanical impacts of neighbouring teeth during the power stroke kinematics of occluding teeth experiencing two- or three-body interactions. Regarding the latter limit, further work on the subject is in progress.

Despite those limitations, we think that our approach shows in principle how the simulation of tooth biomechanics can be advanced considering individual wear patterns. This pilot study can only be understood as a starting point for further discussions. We are, however, convinced that advanced loading concepts that are derived from an evaluation of the kinematics of teeth interaction – namely, an evaluation of the occlusal wear-pattern of an individual tooth – will provide substantially more insights into the detailed functional aspects of dental features such as crests and grooves, enamel thickness and root morphology.

Acknowledgements

This research was supported by the Deutsche Forschungsgemeinschaft (DFG, German Research Foundation) and is publication no. 29 of the DFG Research Unit 771 'Function and performance enhancement in the mammalian dentition – phylogenetic and ontogenetic impact on the masticatory apparatus'. This work was supported by NSF 01-120 Hominid Grant 2007.

Authors' contributions

Dr Stefano Benazzi: concept/design, acquisition of data, data analysis (OFA and FEA), data interpretation, drafting of the manuscript. Dr Ottmar Kullmer: contributions to concept/design, data analysis (OFA), data interpretation, drafting of the manuscript. Prof. Dr Ian R. Grosse: data analysis (FEA), data interpretation, critical revision of the manuscript and approval of the article. Prof. Dr Gerhard W. Weber: contributions to concept/design, critical revision of the manuscript and approval of the article.

References

Acsàdi G, Nemeskéri J (1970) *History of Human Life Span and Mortality*. Budapest: Akadémiai Kiadò.

Ateş M, Çilingir A, Sülün T, et al. (2006) The effect of occlusal contact localization on the stress distribution in complete maxillary denture. *J Oral Rehabil* **33**, 509–513.

Buikstra JE, Ubelaker DH (1994) *Standards for Data Collection from Human Skeletal Remains*. Research Series, no. 44. Fayetteville: Arkansas Archaeological Survey.

Cheng YY, Li JY, Fok SL, et al. (2010a) 3D FEA of high-performance polyethylene fiber reinforced maxillary dentures. *Dent Mater* **26**, 211–219.

Cheng YY, Cheung WL, Chow TW (2010b) Strain analysis of maxillary complete denture with three-dimensional finite element method. *J Prosthet Dent* **103**, 309–318.

Chowdhary R, Lekha K, Patil NP (2008) Two-dimensional finite element analysis of stresses developed in the supporting tissues under complete dentures using teeth with different cusp angulations. *Gerodontology* **25**, 155–161.

Coelho PG, Silva NR, Thompson VP, et al. (2009) Effect of proximal wall height on all-ceramic crown core stress distribution: a finite element analysis study. *Int J Prosthodont* **22**, 78–86.

Cook RD, Malkus DS, Plesha ME, et al. (2002) *Concepts and Applications of Finite Element Analysis*, 4th edn. New York: Wiley & Sons.

De Jager N, Pallav P, Feilzer AJ (2005) The influence of design parameters on the FEA-determined stress distribution in CAD–CAM produced all-ceramic dental crowns. *Dent Mater* **21**, 242–251.

De Jager N, de Kler M, van der Zel JM (2006) The influence of different core material on the FEA-determined stress distribution in dental crowns. *Dent Mater* **22**, 234–242.

Dejak B, Młotkowski A, Romanowicz M (2003) Finite element analysis of stresses in molars during clenching and mastication. *J Prosthet Dent* **90**, 591–597.

Dejak B, Mlotkowski A, Romanowicz M (2005) Finite element analysis of mechanism of cervical lesion formation in simulated molars during mastication and parafunction. *J Prosthet Dent* **94**, 520–529.

Dejak B, Mlotkowski A, Romanowicz M (2007) Strength estimation of different designs of ceramic inlays and onlays in molars based on the Tsai-Wu failure criterion. *J Prosthet Dent* **98**, 89–100.

DeLong R (2006) Intra-oral restorative materials wear: rethinking the current approaches: how to measure wear. *Dent Mater* **22**, 702–711.

Every RG (1972) *A New Terminology for Mammalian Teeth: Founded on the Phenomenon of Thegosis*, Parts 1 and 2. Christchurch: Pegasus.

Ferenbach D, Schwidetzky I, Stloukal M (1980) Recommendations for age and sex diagnosis of skeletons. *J Hum Evol* **9**, 517–550.

Fernandes CP, Glantz P-OJ, Svensson SA, et al. (2003) Reflection photoelasticity: a new method for studies of clinical mechanics in prosthetic dentistry. *Dent Mater* **19**, 106–117.

Fiorenza L, Benazzi S, Tausch J, et al. (2010) Brief communication: identification reassessment of the isolated tooth Krapina D58 through occlusal fingerprint analysis. *Am J Phys Anthropol* **143**, 306–312.

Fu G, Deng F, Wang L, et al. (2010) The three-dimension finite element analysis of stress in posterior tooth residual root restored with postcore crown. *Dent Traumatol* **26**, 64–69.

Goel VK, Khera SC, Ralston JL, et al. (1991) Stresses at the dentinoenamel junction of human teeth – a finite element investigation. *J Prosthet Dent* **66**, 451–459.

Gurbuz T, Sengul F, Altun C (2008) Finite element stress analysis of short-post core and over restorations prepared with different restorative materials. *Dent Mater J* **27**, 499–507.

Hasegawa A, Shinya A, Nakasone Y, et al. (2010) Development of 3D CAD/FEM analysis system for natural teeth and jaw bone constructed from X-Ray CT images. *Int J Biomater*, doi:10.1155/2010/659802.

Hattori Y, Satoh C, Kunieda T, et al. (2009) Bite forces and their resultants during forceful intercuspation clenching in humans. *J Biomech* **42**, 1533–1538.

Hiiemae KM, Kay RF (1972) Trends in the evolution of primate mastication. *Nature* **240**, 486–487.

Hillson S (2003) *Dental Anthropology*. Cambridge: Cambridge University Press.

Holmes DC, Diaz-Arnold AM, Leary JM (1996) Influence of post dimension on stress distribution in dentin. *J Prosthet Dent* **75**, 140–147.

Jiang W, Bo H, YongChun G, et al. (2010) Stress distribution in molars restored with inlays or onlays with or without endodontic treatment: a three-dimensional finite element analysis. *J Prosthet Dent* **103**, 6–12.

Kaidonis JA (2008) Tooth wear: the view of the anthropologist. *Clin Oral Invest* **12**, 21–26.

Kaidonis JA, Townsend GC, Richards LC (1993) Nature and frequency of dental wear facets in an Australian Aboriginal population. *J Oral Rehabil* **20**, 333–340.

Kay RF (1977) The evolution of molar occlusion in the Cercopithecidae and early catarrhines. *Am J Phys Anthropol* **46**, 327–352.

Kay RF, Hiiemae KM (1974) Jaw movement and tooth use in recent and fossil primates. *Am J Phys Anthropol* **40**, 227–256.

Ko CC, Chu CS, Chung KH, et al. (1992) Effects of posts on dentin stress distribution in pulpless teeth. *J Prosthet Dent* **68**, 421–427.

Kondo T, Wakabayashi N (2009) Influence of molar support loss on stress and strain in premolar periodontium: a patient-specific FEM study. *J Dent* **37**, 541–548.

Kullmer O, Benazzi S, Fiorenza L, et al. (2009) Technical note: occlusal fingerprint analysis: quantification of tooth wear pattern. *Am J Phys Anthropol* **139**, 600–605.

Kupczik K, Hublin JJ (2010) Mandibular molar root morphology in Neanderthals and Late Pleistocene and recent *Homo sapiens*. *J Hum Evol* **59**, 525–541.

Li H, Zhou ZR (2002) Wear behavior of human teeth in dry and artificial saliva conditions. *Wear* **249**, 980–984.

Lucas PW (2004) *Dental Functional Morphology. How Teeth Work*. Cambridge: Cambridge University Press.

Macho GA, Spears IR (1999) Effects of loading on the biochemical behaviour of molars of Homo, Pan, and Pongo. *Am J Phys Anthropol* **109**, 211–227.

Magne P (2007) Efficient 3D finite element analysis of dental restorative procedures using micro-CT data. *Dent Mater* **23**, 539–548.

Maier W, Schneck G (1981) Konstruktionsmorphologische Untersuchungen am Gebiß der hominoiden Primaten. *Z Morphol Anthrop* **72**, 127–169.

Molnar S, Ward SC (1977) On the hominid mastleatory complex: biomechanical and evolutionary perspectives. *J Hum Evol* **6**, 557–568.

Nishigawa G, Matsunaga T, Maruo Y, et al. (2003) Finite element analysis of the effect of the bucco-lingual position of artificial posterior teeth under occlusal force on the denture supporting bone of the edentulous patient. *J Oral Rehabil* **30**, 646–652.

Palamara D, Palamara JEA, Tyas MJ, et al. (2000) Strain patterns in cervical enamel of teeth subjected to occlusal loading. *Dent Mater* **16**, 412–419.

Palamara JEA, Palamara D, Messer HH (2002) Strains in the marginal ridge during occlusal loading. *Aust Dent J* **47**, 218–222.

Picton DCA (1962) Tilting movements of teeth during biting. *Arch Oral Biol* **7**, 151–159.

Prombonas A, Vlissidis D (2002) Effects of the position of artificial teeth and load levels on stress in the complete maxillary denture. *J Prosthet Dent* **88**, 415–422.

Rafferty BT, Janal MN, Zavanelli RA, et al. (2010) Design features of a three-dimensional molar crown and related maximum principal stress. A finite element model study. *Dent Mater* **26**, 156–163.

Reeh ES, Douglas WH, Levine MJ (1995) Lubrication of human and bovine enamel compared in an artificial mouth. *Arch Oral Biol* **40**, 1063–1072.

Roy S, Basu B (2008) Mechanical and tribological characterization of human tooth. *Mater Charact* **59**, 747–756.

Rubin C, Krishnamurthy N, Capilouto E, et al. (1983) Stress analysis of the human tooth using a three-dimensional finite element model. *J Dent Res* **62**, 82–86.

Schwartz GT (2000) Taxonomic and functional aspects of the patterning of enamel thickness distribution in extant large-bodied hominoids. *Am J Phys Anthropol* **111**, 221–244.

Smith BH (1984) Patterns of molar wear in hunter-gatherers and agriculturists. *Am J Phys Anthropol* **63**, 39–56.

Spears IR, Macho GA (1998) Biomechanical behaviour of modern human molars: implications for interpreting the fossil record. *Am J Phys Anthropol* **106**, 467–482.

Spoor F, Zonneveld F, Macho GA (1993) Linear measurements of cortical bone and dental enamel by computed tomography: applications and problems. *Am J Phys Anthropol* **91**, 469–484.

Turteltaub MJ, Sternberg E (1968) On concentrated loads and green's functions in elastostatics. *Arch Ration Mech Anal* **29**, 193–240.

Ulhaas L, Kullmer O, Schrenk F, et al. (2004) A new 3-d approach to determine functional morphology of cercopithecoid molars. *Ann Anat* **186**, 487–493.

Ulhaas L, Kullmer O, Schrenk F (2007) Tooth wear diversity in early hominid molars: a case study. In: *Dental Perspectives on Human Evolution: State of the Art Research in Dental Paleoanthropology* (eds Bailey SE, Hublin JJ), pp. 369–390. Dordrecht: Springer.

Wall CE, Vinyard CJ, Johnson KR, et al. (2006) Phase II jaw movements and masseter muscle activity during chewing in *Papio anubis*. *Am J Phys Anthropol* **129**, 215–224.

Zheng J, Zhou ZR (2006) Effect of age on the friction and wear behaviors of human teeth. *Tribol Int* **39**, 266–273.

Zheng J, Zhou ZR (2007) Friction and wear behavior of human teeth under various wear conditions. *Tribol Int* **40**, 278–284.